

A comparative analysis of ANFIS and fuzzy controllers for a dynamic hybrid model

Laoufi Kaltoum¹, Youssef Mouloudi², Abdeldjebar Hazzab¹, Abdallah Ben Abdelkader²

¹Laboratory of Command, Analysis and Optimization of Electro-Energetic Systems, University of Bechar, Béchar, Algeria

²Laboratory of Smart Grids and Renewable Energies (S.G.R.E), Department of Electrical Engineering, Faculty of Technology, University of Bechar, Béchar, Algeria

Article Info

Article history:

Received Jun 7, 2024

Revised Oct 14, 2024

Accepted Oct 23, 2024

Keywords:

ANFIS

Battery model

Fuzzy

Hybrid fuel cell vehicle

intelligent control

Proportional integral derivative

Sim Power Systems

ABSTRACT

Transitioning from combustion engines to electric motors is essential to reduce CO₂ emissions and combat climate change. This study presents a dynamic hybrid model combining a fuel cell and battery for electric vehicles, emphasizing simplified parameter extraction from battery datasheets. The model integrates two energy storage systems: batteries for electrochemical storage and hydrogen for chemical storage, converted into electricity via a fuel cell stack. This dual approach enables flexible refueling options with electricity or hydrogen. An air compressor in the proton exchange membrane (PEM) fuel cell stack optimizes performance across varying driving conditions. The research aims to minimize fuel cell consumption and enhance energy storage efficiency using Sim Power Systems software. It employs traditional proportional integral derivative (PID) controllers and advanced optimization techniques, including fuzzy and adaptive neuro-fuzzy inference system (ANFIS), to achieve optimal power distribution between the fuel cell system (FCS) and the energy secondary source (ESS) for specific road scenarios. The proposed ANFIS-based approach demonstrates superior control in balancing energy efficiency and driving dynamics, surpassing both PID and fuzzy logic controllers in key metrics. This innovative closed-loop control system offers a promising solution for hybrid electric vehicles, ensuring optimal performance and energy management.

This is an open access article under the [CC BY-SA](https://creativecommons.org/licenses/by-sa/4.0/) license.



Corresponding Author:

Abdallah Ben Abdelkader

Laboratory of Smart Grids and Renewable Energies (S.G.R.E), Department of Electrical Engineering

Faculty of Technology, University of Bechar

Béchar, Algeria

Email: benabdelkader.abdellah@univ-bechar, abdallahbenabdelkader@yahoo.fr

1. INTRODUCTION

In light of the growing concern over dwindling fossil fuel reserves and escalating global energy requirements, hydrogen emerges as a promising energy carrier to supplant traditional fuels in the long run. As the most abundant element in the universe with non-toxic byproducts, hydrogen presents itself as an environmentally friendly option, particularly when utilized through a fuel cell hydrogen vehicle (FCHV). The advent of electric vehicles equipped with energy storage systems (ESS) marks a significant step towards establishing a fleet of clean transportation methods. Although current battery technologies offer only about 10% of the energy density of conventional fuels [1]-[3], fuel cells (FCs) with their high energy density stand out as an ideal complementary energy storage solution for clean vehicles [1], [2]. The conversion of hydrogen (H₂) into electricity via fuel cells represents a pivotal electrochemical process, offering a clean alternative to traditional thermal combustion methods. While fuel cells have been in existence since their

discovery in 1839, their widespread adoption faces several technical and economic obstacles that need to be addressed before mass commercialization can occur. Challenges such as battery costs, FCS integration, and hydrogen production and storage need to be overcome to realize the full potential of this technology. This study focuses on addressing the power selection for the fuel cell system and secondary energy source in a hybrid FCHV. A dimensioning tool is proposed to ensure compliance with specified dynamic performance requirements of the vehicle along with an energy criterion, such as hydrogen consumption. The methodology is exemplified through an application on a prototype hybrid FCHV, considering the unique current/voltage characteristics of fuel cells and their impact on system performance. The research shifts towards controlling a fuel cell energy system for residential applications, with a specific emphasis on proton exchange membrane cells (PEM). Known for their suitability in the automotive and decentralized electric power generation sectors, PEM cells offer rapid dynamics and operate at relatively low temperatures, simplifying integration into various systems. This study aims to delve into the physicochemical phenomena within PEMFC cells to optimize performance and facilitate seamless integration into energy production systems.

Utilizing adaptive neuro-fuzzy inference system (ANFIS), this research endeavors to construct a versatile model for intricate systems. Subsequently, a dynamic model of a fuel cell energy system for residential use is outlined, encompassing a cell model, gas reformer model, and power processing unit. The proposed model includes strategies for controlling cell power, emphasizing the integration of ANFIS and fuzzy logic for system modeling and control.

The paper is structured as follows: i) Section 1 introduces the PEM fuel cell; ii) Section 2 elaborates on the polymer membrane fuel cell (PMFC) system; iii) Section 3 discusses hybrid fuel cell vehicles (FCHV); iv) Section 4 describes electric vehicle systems; v) Section 5 scrutinizes various control methodologies (PID, fuzzy, ANFIS) through tests on the proposed model; and vi) Section 6 consolidates the simulation results of the different test cases. In conclusion, this study aims to offer insights into the modeling and control of fuel cell systems while highlighting the effectiveness of ANFIS and fuzzy logic approaches across diverse domains, particularly in system identification and control.

2. THE POLYMER MEMBRANE FUEL CELL SYSTEM (FCS)

2.1. Working principle

The FCS fuel cell transforms chemical energy (hydrogen and oxygen) into electrical energy. This electrochemical process represents the reverse electrolysis of water [4]. Electrical energy is generated by a redox process with oxygen as the oxidant and hydrogen as the reducer. Oxidation occurs at the anode, whereas reduction transpires at the cathode. Both processes are separated by a membrane functioning as an electrolyte. The cathode receives gaseous oxygen (or, more broadly, air), whereas the anode is provided with gaseous hydrogen. Electricity is generated by the two electrons emitted from the hydrogen molecule (Figure 1). The H^+ hydrogen protons traverse the membrane dividing the anode from the cathode, recombining with electrons and oxygen atoms at the cathode. Ideally, the sole byproducts of the reaction are water and heat. Figure 1 elucidates the concept of the PEM fuel cell.

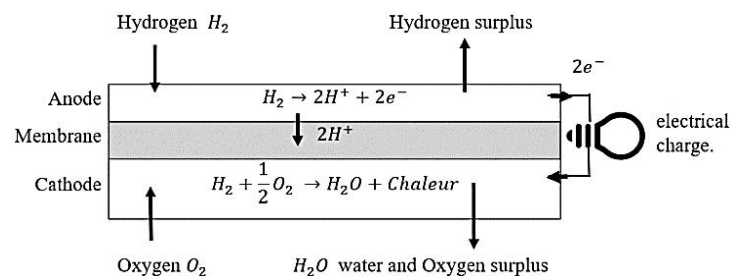


Figure 1. PEM fuel cell block diagram [4]

2.2. The electrical characteristic of the fuel cell

The role of the electrochemical potential in the redox process. The optimal electrochemical potential is 1.23 V (standard potential) at standard temperature and pressure conditions (1 atm, 25 °C). In reality, the open-circuit voltage is somewhat under 1 V [5]. The electrical property of a fuel cell is referred to as the polarization curve. The cell's voltage is depicted as a function of current density. The membrane's humidity, operating temperature, and reagent pressure determine it. i_{PAC} (A/cm²) represents the current density.

$$i_{PAC} = \frac{I_{PAC}}{A_{cell}} \quad (1)$$

With i_{PAC} the current of the fuel cell and A_{cell} the active surface of a membrane.

2.3. Fuel cell system for vehicle

Figure 1 illustrates the four subsystems of a fuel cell vehicle system: the airflow supply system for the cathode, the hydrogen flow supply system for the anode, the cooling system, and the humidification system. The airflow supply subsystem comprises a compressor, cooler, water separator, back pressure valve, connecting pipes, and additional components, facilitating the delivery of essential airflow to the stack cathode. The hydrogen flow supply subsystem includes a hydrogen tank, a solid valve, a recirculation pump, a purge valve, and connecting pipes, along with additional components. The purpose of this mechanism is to ensure that the stack anode is supplied with adequate hydrogen. The air temperature will rise during compression, necessitating the use of an air cooler to reduce the temperature before reaching the stack. A humidifier is utilized to improve proton conductivity by adding moisture to the airflow. On the cathode side of the stack, an electrochemical reaction occurs between oxygen and protons, resulting in the formation of water and the release of heat. The introduction of coolant into the pile is essential for heat dissipation, followed by its expulsion into the atmosphere through a radiator to maintain the stack temperature within acceptable limits. The water separator removes moisture from the exhaust air stream. The back pressure valve regulates the airflow pressure within the stack to ensure it remains at an optimal level.

A variety of fuel cell models have been developed for different applications [6], [7], with the models described in [8]-[10] categorized as control-oriented models. The fuel cell system model utilized in this study incorporates a twin-screw compressor, as cited in references [8], [9], and [11]. A twin-screw compressor offers multiple benefits when compared to a centrifugal compressor:

- Its nominal rotational speed is approximately an order of magnitude lower than that of a centrifugal compressor, leading to a more reliable system;
- The flow curve in the compressing map is almost linear at a constant velocity and is less affected by pressure compared to a centrifugal compressor, hence facilitating system control; and
- A twin-screw compressor does not encounter the "surge" phenomena, hence streamlining the control system. The compressor map and twin-screw compressor models are derived from [11] and [12]. Figure 2 depicts the twin-screw compressor concept, which is divided into two pieces. The static compressor map is the initial component that determines the airflow rate and compressor power. The subsequent phase involves implementing modifications. Due to the disparity between a compressor's operational environment and its testing conditions, its airflow and energy must be modified in accordance with thermodynamic principles. The model P_{amb} is tested using inputs of downstream pressure P_{sm} , rotational speed N_{CP} , air pressure P_{atm} , pressure P_0 (1.013 bar), and temperature T^0 (293.15 K). Compressor motor torque and power are required to ascertain rotational speed. The compressor is connected to the supply manifold, and its downstream pressure corresponds to the pressure in the supply manifold, as dictated by the downstream cathode flow field.

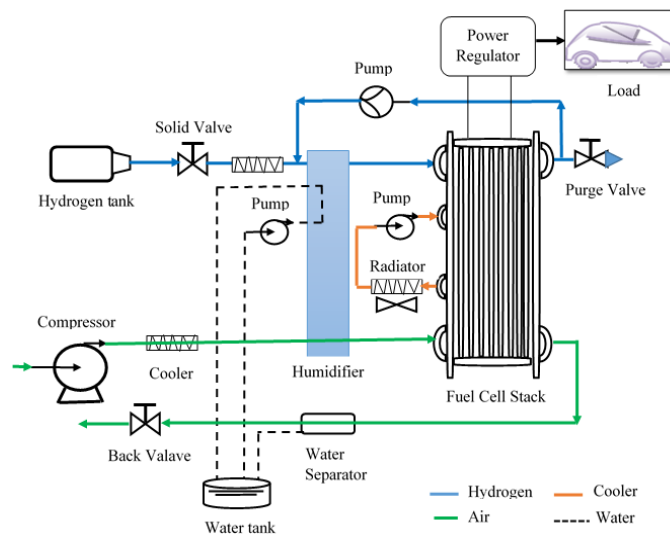


Figure 2. The architecture of a fuel cell system for vehicle [13]

The compressor's rotation speed may index the compressor power P_{cp} from the compressor power P_{amb} . The compressor flow P_{amb} determines the airflow rate W_{cp} by using the compression ratio and rotation speed. The revised air flow rate, W_{cp_re} , is then computed using (2).

$$W_{cp_re} = \frac{T_{amb}}{T_0} \times \frac{P_0}{P_{amb}} W_{cp} \quad (2)$$

With the formulae given in [9], the air temperature exiting the compressor T_{cp} is determined.

The hydrogen fuel consumption of PEMFC is determined by (2) [14]. Load power variations and repetitive start-stop cycles represent two significant challenges that negatively impact the performance and longevity of fuel cell systems [15]. The identified issues result in substantial complications, such as membrane drying and water flooding, which may cause irreversible damage to the channel and gas diffusion layers [16].

$$M_{H_2} = \int_0^t \frac{V_{FC}(t) i_{FC}(t)}{\eta_{dc}(t) \rho_{H_2}} dt \quad (3)$$

In the computation model, the reference value of the air flow W_{cp}^* is calculated as in [17].

$$W_{cp}^* = \left[1 + \frac{M_V \phi_{atm} P_{Sat}^{atm}}{M_a^{atm} (P_{atm} - \phi_{atm} P_{Sat}^{atm})} \right] \frac{1}{\gamma_{O_2}} \lambda_{best} M_{O_2} \frac{nI_{st}}{4F} \quad (4)$$

Where ϕ_{atm} is air relative humidity; P_{Sat}^{atm} is the vapor saturation pressure with relative humidity ϕ_{atm} ; P_{atm} is atmospheric pressure; M_V is the molar mass of vapor; M_a^{atm} is the air molar mass with relative humidity ϕ_{atm} ; M_{O_2} is oxygen molar mass; n is the number of single fuel cells; F is Faraday's constant; and γ_{O_2} is oxygen mass fraction in the air, calculated by: $\gamma_{O_2} = 0.21 \frac{M_{O_2}}{M_a^{atm}}$.

To model the concentration of oxygen in the cathode, we first define a parameter called the oxygen excess ratio λ_{O_2} .

$$\lambda_{O_2} = \frac{W_{O_2_in}}{W_{O_2_rct}} \quad (8)$$

Where $W_{O_2_in}$ is the flow of oxygen into the cathode and $W_{O_2_rct}$ is the mass of oxygen reacted in the cathode; low values of λ_{O_2} indicate low oxygen concentration in the cathode or oxygen starvation. The rate of oxygen reacted $W_{O_2_rct}$ depends on the current drawn from the stack I_{st} . The mass flow rate out of the supply manifold W_{sm} , depends on the downstream (cathode) pressure.

$$W_{O_2_rct} = M_{O_2} \frac{nI_{st}}{4F} \quad (9)$$

$$W_{O_2_in} = \gamma_{O_2} \frac{1}{1 + \phi_{atm}} W_{sm} \quad (10)$$

3. HYBRID FUEL CELL VEHICLE (FCHV)

The vehicle's electrical power system, as seen in Figure 3, comprises the electrical machine, the secondary power source, and the fuel cell system. To integrate these components into one or several buses, it is essential to establish an electrical architecture. The electric machine is methodically outfitted with a converter to facilitate torque management. The converter is reversible in power to give the necessary energy during the traction phases and to recover the energy provided by the electric machine during the vehicle braking phases.

At the power source level, a primary function of the power converter(s) is to regulate the power distribution between the PAC system and the auxiliary energy source. Furthermore, its local control often enables the regulation of current, voltage, and/or power transferred to safeguard the linked devices [18], [19]. Incorporate a variable into the power allocation process: Hybridization enables the distribution of power demand between the fuel cell system and the auxiliary energy source. This enables the modification of the operational parameters of the FCS system to optimize performance in higher yield areas through effective management strategies, consequently decreasing hydrogen consumption. Within the powertrain of a hybrid fuel cell vehicle, multiple operational modes can be delineated. The operational modes of traction, braking, and halting generate distinct energy flows.

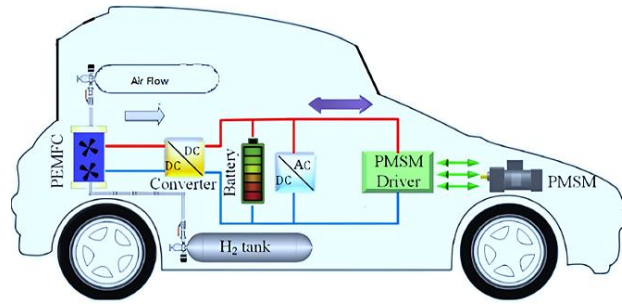


Figure 3. Example of hybrid fuel cell vehicle architecture

3.1. The secondary source of energy

The main feature of the secondary energy source is its ability to reverse the power generation process. The secondary source may be replenished through kinetic energy recovery or by utilizing the fuel cell. A battery functions as an electrochemical energy converter, enabling the chemical storage of energy. The primary technologies utilized in hybrid automobiles include lead-acid batteries, nickel metal-hydrate (Ni-MH), and lithium-ion (Li-ion) [20]. Nickel-metal hydrate (Ni-MH) technology is widely recognized for its advantageous characteristics in terms of capacity, lifespan, and economic efficiency. Li-ion technology demonstrates high specific power (W/kg) and specific capacity (Wh/kg); however, improvements are necessary regarding cost, operational safety, service life, and low-temperature performance. The primary technology exhibits a low specific capacity due to the significant weight of the batteries; however, it remains a robust and economical choice that benefits from ongoing advancements [21], [22].

4. CONTROL STRATEGIES

4.1. Adaptive neuro-fuzzy inference system (ANFIS)

The ANFIS model exemplifies a sophisticated method for enhancing Takagi Sugeno fuzzy inference systems, which are recognized as the most widely utilized framework in practical applications. The architecture utilizes multilayer networks, formed by cells that perform designated duties while conforming to established criteria [18], [19]. To exemplify the fundamental idea of ANFIS, we examine a fuzzy inference system with two inputs (x , y), and a singular output z , as seen in the schematic in Figure 4. This framework effectively combines neural network flexibility with fuzzy logic accuracy, providing a robust instrument for intricate system modeling and optimization.

The parameters of the ANFIS system are classified as premise membership function parameters and consequent parameters. The learning process employs a hybrid methodology: the gradient descent algorithm optimizes the premise parameters, while the least-squares approach accurately computes the consequent parameters. This cooperative learning method enhances the model's accuracy and adaptability. The operational framework of the ANFIS system may be outlined as follows:

$$\text{Rule } i: \text{ if } x \text{ is } A_i; \text{ and } y \text{ is } B_i; \text{ then } z_i = p_i x + q_i y + r_i$$

where A_i and B_i represent the fuzzy sets associated with the function node. As in Figure 4, the ANFIS is composed of five layers.

- Layer 1: Each node i in this layer uses a membership function given by: $o_i^1 = \mu_{A_i}(x)$. Where x is the input for node i (same for input y , $o_i^1 = \mu_{B_i}(y)$). μ_{A_i} represents the membership function of A_i and it specifies the degree of membership with which x satisfies. Generally, $\mu_{A_i}(x)$ is chosen as a Gaussian function.

$$\mu_{A_i}(x) = \exp \left[-\frac{(x - c_i)^2}{\sigma_i} \right] \quad (11)$$

With c_i , σ_i are parameters that refer to the premise parameters. The values of these last changes according to various exhibitions of the function of belonging.

- Layer 2: The outputs of this layer are the weights of the rules, which are obtained by a simple multiplication of the entries in each cell. multiplication of the entries in each cell.

$$o_i^2 = \mu_{A_i}(x) \times \mu_{B_i}(y) \quad (12)$$

- Layer 3: This layer corresponds to the normalization of rule weights by the relationship.

$$o_i^3 = \bar{w}_i = \frac{w_i}{w_1+w_2}, i = 1,2 \tag{13}$$

- Layer 4: Each node i in this layer is a node that is calculated as (14).

$$o_i^4 = \bar{w}_i z_i = \bar{w}_i(p_i x + q_i y + r_i) \tag{14}$$

Where \bar{w}_i are the outputs of layer 3 and (p_i, q_i, r_i) are the consequent parameters of the output function.

- Layer 5: The single node in this layer sums all the input signals and returns, as output, the approximate value of the desired function expressed by (15).

$$o_i^5 = \sum_i \bar{w}_i z_i = \frac{\sum_{i=1}^2 w_i z_i}{\sum_{i=1}^2 w_i} \tag{15}$$

ANFIS design integrates input parameters and generates subsequent parameters, represented as a linear combination in the output.

$$z = \frac{w_1}{w_1+w_2} z_1 + \frac{w_2}{w_1+w_2} z_2 = \bar{w}_1 z_1 + \bar{w}_2 z_2 = (\bar{w}_1 x) p_1 + (\bar{w}_1 y) q_1 + (\bar{w}_1) r_1 + (\bar{w}_2 x) p_2 + (\bar{w}_2 y) q_2 + (\bar{w}_2) r_2 \tag{16}$$

With $p_i, q_i,$ and r_i are linear consequential parameters.

The gradient descent method optimizes the premise parameters, while the consequent parameters are determined using the least-squares technique. This approach ensures the optimal identification of the resultant parameters, provided the premise parameters stay unchanged. A balance between computational complexity and performance results dictates the selection of these tactics. Consequently, the hybrid learning approach outperforms solitary gradient descent in efficacy and facilitates the segmentation of the parameter set for optimized computation [23].

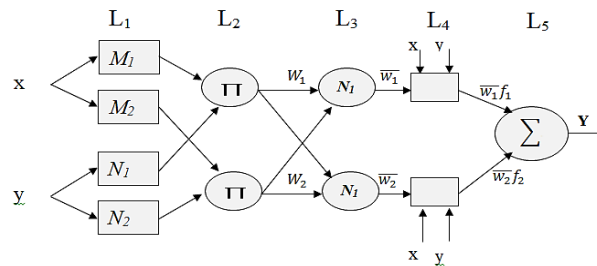


Figure 4. Architecture of ANFIS controller

5. THE SIMULATION RESULTS AND DISCUSSION

Figure 5 presents a the vehicle's power requirements dynamic hybrid model combining a fuel cell and battery for electric vehicles to create a multi-domain simulation of a fuel cell vehicle (FCV) drivetrain. Nevertheless, a commonly employed fuel cell vehicle (FCV) powertrain is exemplified by the Honda Clarity [24]. The electric motor is energized by a fuel cell and a battery to function the fuel cell vehicle (FCV). The electric motor, battery, fuel cell, and DC/DC converter are the four components of the FCV electrical subsystem. Where the electric motor is a 100-kW internal permanent magnet synchronous machine functioning at a supply voltage of 288 VDC. This motor incorporates integrated magnets and contains eight poles. Flux vector control is essential to achieve a maximum motor speed of 12,500 rpm.

Parameters Sim Power Systems the fuel cell stack has 400 cells, delivering a peak output of 90 kW. A supplementary source that provides more power when required is a 13.9 Ah, 288 VDC, 25 kW lithium-ion battery [24], [25]. We desire clarity in Figure 6 to illustrate the multiple working modes of the FCV during a whole cycle, namely: acceleration, cruising, recharging the battery during acceleration, and regenerative braking. The simulated operation time in acceleration mode is roughly one minute. The FCV accelerates from 0 km/h to around 90 km/h in 12 seconds, thereafter decelerating to 80 km/h in 16 seconds. This exceptional outcome is achieved by maintaining the accelerator pedal at 70% for the initial 4 seconds, followed by 25% for the subsequent 4 seconds after complete release, and then at 85% when the pedal is re-engaged. Pressure is applied for 4 seconds, then a brake setting of -70% is set until the end of the exercise.

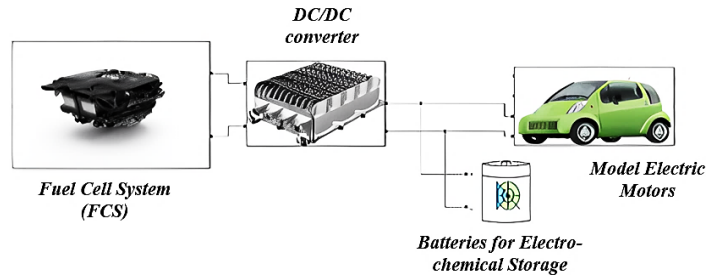


Figure 5. Multi-domain simulation of an FCV power train based on Sim Power Systems and Sim Driveline [24]

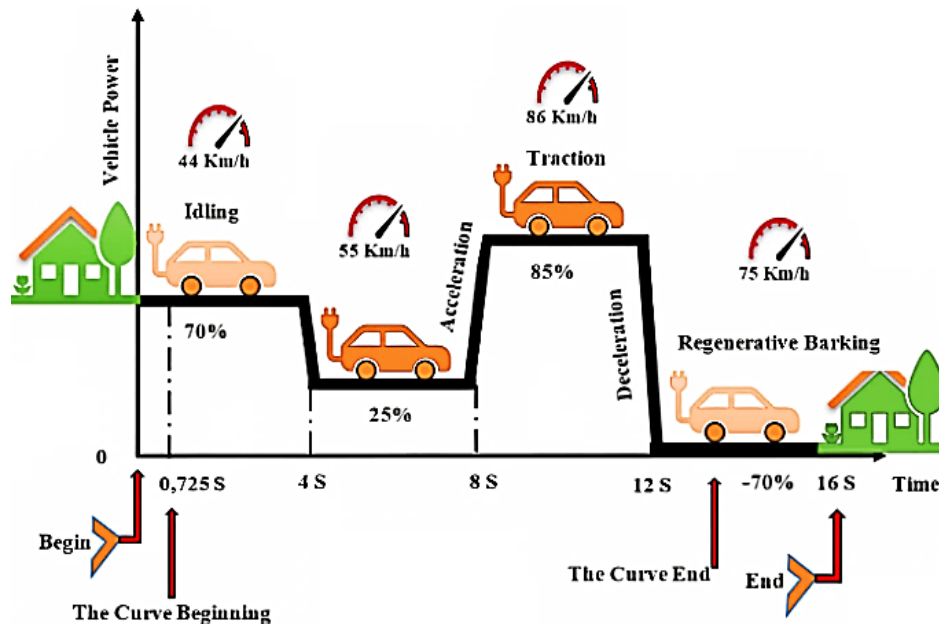


Figure 6. Specify driving road topology

The following illustrates what occurs when the FCV moves: initially, at time $t = 0$ seconds, the fuel cell vehicle (FCV) is at rest, and the driver engages the accelerator pedal to 70% of its capacity, relying on the battery to power the engine until the fuel cell is activated. Starting at $t = 0.725$ seconds, the vehicle's speed gradually increases from 0 km/h to 44 km/h. However, the fuel cell is unable to reach the reference power because of its large time constant, requiring ongoing battery assistance. At $t = 4$ seconds, when the accelerator pedal is released to 25%, the fuel cell is unable to promptly decrease its power output, resulting in the battery supplying the required torque to sustain a constant speed of 55 km/h. Figure 7 shows the change in values representing the speed of the car from take-off to arrival, as the graphs show the dynamic response of the fuel cell and battery system. Figure 7(a) illustrates the fuel cell output power lagging behind demand, while Figure 7(b) shows the vehicle speed stabilizing at 55 km/h. Figure 7(c) presents a gradual depletion of the battery state of charge, and Figure 7(d) demonstrates the torque output, highlighting how the battery supports the fuel cell during changes in accelerator input.

At $t = 6$ seconds, following a duration of two minutes, the power output of the fuel cell aligns with the reference power, rendering the battery unnecessary. At $t = 8$ seconds, the driver accelerates by pressing the accelerator pedal to 85%, causing the fuel cell system to function at a speed of 86 km/h, with the battery providing supplementary power. At $t = 8.05$ seconds, the combined output from the fuel cell and battery is insufficient to meet the required demand, leading to a torque mismatch, attributed to the fuel cell's response time. At $t = 8.45$ seconds, the observed torque aligns with the reference value due to the increase in fuel cell power, resulting in a decrease in battery power to 9 kW. Figure 8 shows the motor speed. Figure 8(a) demonstrates the fuel cell power achieving the reference level, whereas Figure 8(b) depicts the stabilization of vehicle speed at 86 km/h. Figure 8(c) illustrates the reduction in battery power as it supports the fuel cell, while Figure 8(d) emphasizes the torque output following the reference.

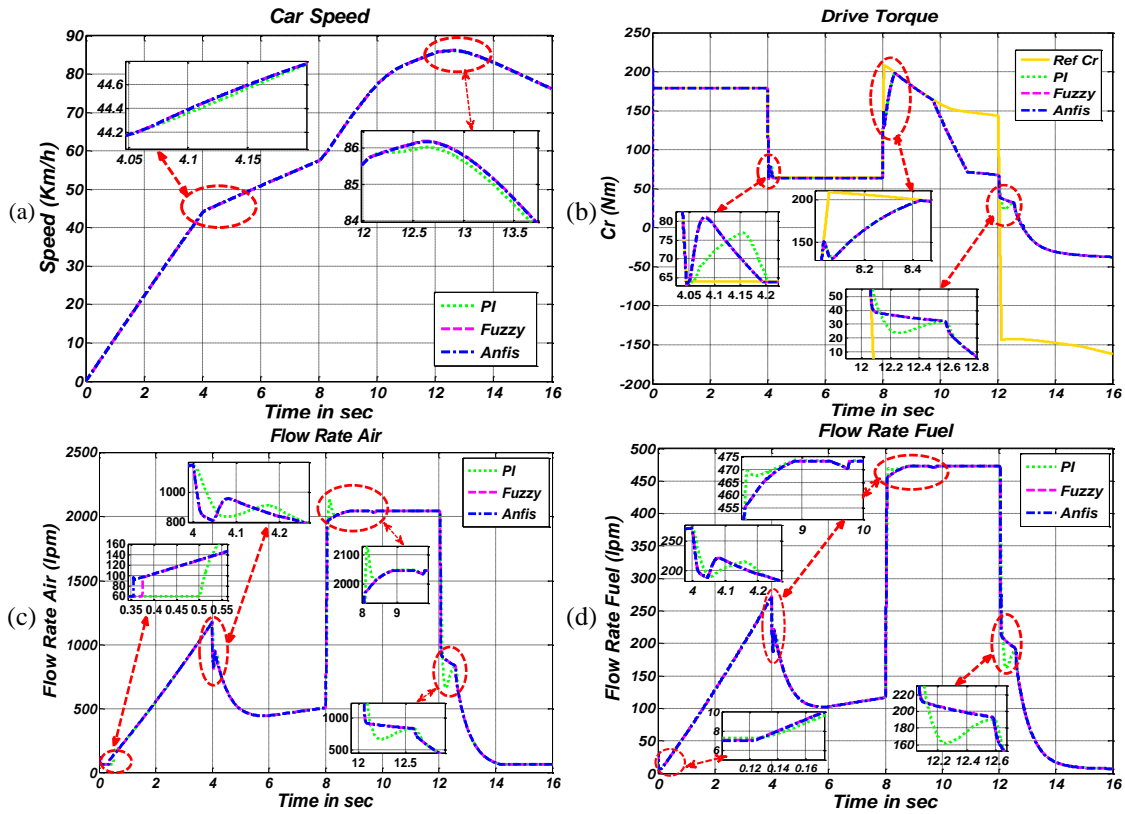


Figure 7. The change in values represents the speed of the car from take-off to arrival: (a) car speed, (b) drive torque, (c) flow rate air, and (d) flow rate fuel

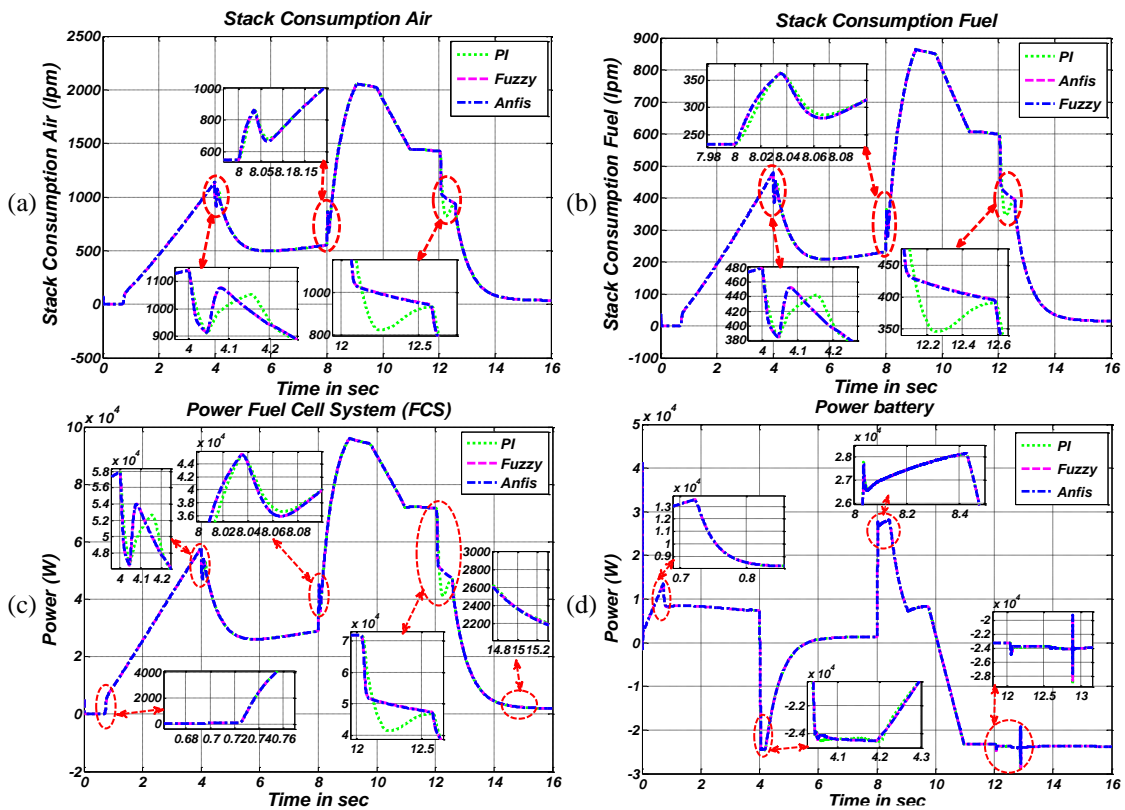


Figure 8. The motor speed shows (a) stack consumption air, (b) stack consumption fuel, (c) power fuel cell system, and (d) power battery

At $t = 10.9$ seconds, the battery's state of charge (SOC) decreases to 39.99%, requiring recharging due to its fall below the 40% threshold. The fuel cell manages the distribution of energy between the battery and the engine, enabling the battery to draw a maximum of -24 kW. In this phase, the battery is recharged while the fuel cell is in operation; however, the necessary torque is not achieved, resulting in a constant motor speed of 86 km/h until $t = 12.8$ seconds. Figure 9 shows the power motor of the fuel cell system (FCS). Figure 9(a) illustrates a decline in state of charge (SOC) below 40%, whereas Figure 9(b) demonstrates a constant vehicle speed. Figure 9(c) depicts the negative battery power during the recharging process, while Figure 9(d) demonstrates the torque output that falls short of meeting the required demand.

At $t = 12$ seconds, the driver modifies the accelerator pedal to -70%, triggering regenerative braking in which the motor functions as a generator. The kinetic energy of the FCV is converted into electrical energy stored in the battery; however, the required torque of -140 Nm cannot be attained because the battery's maximum absorption capacity is limited to 25 kW. The power output of the fuel cell diminishes as a result of its response time, leading to a gradual reduction in vehicle speed from 75 km/h to a complete stop. By $t = 15$ seconds, the fuel cell power attains approximately 2.38 kW, indicating the minimum output. Figure 8(c) illustrates the energy absorption by the battery, Figure 9(a) demonstrates the impact of regenerative braking on power output, Figure 9(b) presents the reduction in vehicle speed, and Figures 8(d) and 9(d) emphasizes the decrease in fuel cell power during this process.

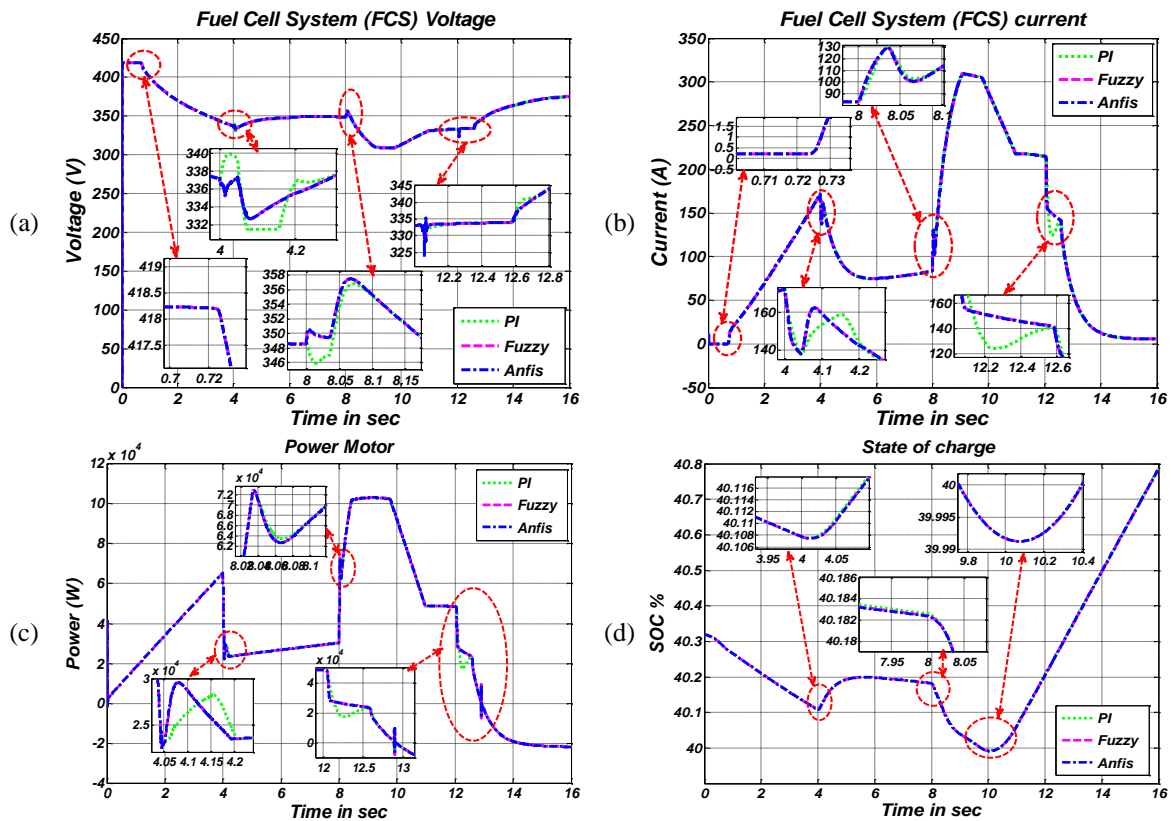


Figure 9: The power motor of (a) FCS voltage, (b) FCS current, (c) power motor, and (d) state of charge

6. CONCLUSION

This paper presents a control-oriented model for proton exchange membrane (PEM) fuel cells, incorporating cathode and anode mass flow transients with a membrane hydration model. The validation of the proposed model required comprehensive testing, resulting in findings that exhibited a high degree of accuracy. Employing this control-centric paradigm, an adaptive neuro-fuzzy inference system (ANFIS) is employed to regulate increased oxygen levels, preventing oxygen deficits and hydrogen flow disruptions during sudden variations in current load inside the fuel cell system.

ANFIS exhibits superiority over conventional PID controllers by amalgamating the benefits of fuzzy logic controllers with those of PID controllers. Comparative simulations demonstrate the efficacy of ANFIS in

managing hydrogen and airflow in PEM fuel cells compared to traditional PID controllers. Due to the sensitivity of fuzzy logic control to system features and load variations, PID parameters are carefully calibrated to enhance system control through rule inference, hence ensuring clarity and precision in control objectives.

Given the critical role of air and hydrogen flow in system performance, ANFIS is an indispensable tool for enhancing control precision. The integration of ANFIS significantly improves control methodologies, leading to superior system performance. In the future, the incorporation of photovoltaic panels in electric vehicles, augmented by supercapacitors for increased electric charge, alongside a sophisticated energy management system employing artificial intelligence, presents the potential for enhanced vehicle efficiency and operational efficacy.




REFERENCES

- [1] H. F. Gharibeh, A. S. Yazdankhah, and M. R. Azizian, "Energy management of fuel cell electric vehicles based on working condition identification of energy storage systems, vehicle driving performance, and dynamic power factor," *Journal of Energy Storage*, vol. 31, p. 101760, Oct. 2020, doi: 10.1016/j.est.2020.101760.
- [2] A. U. Rahman, I. Ahmad, and A. S. Malik, "Variable structure-based control of fuel cell-supercapacitor-battery based hybrid electric vehicle," *Journal of Energy Storage*, vol. 29, p. 101365, Jun. 2020, doi: 10.1016/j.est.2020.101365.
- [3] H. F. Gharibeh, A. S. Yazdankhah, M. Reza Azizian, M. Farrokhifar, and A. Alahyari, "Impact assessment of installed photovoltaic on fuel cell hybrid electric vehicle considering fast identification of power changes," in *2020 International Youth Conference on Radio Electronics, Electrical and Power Engineering (REEPE)*, IEEE, Mar. 2020, pp. 1–6, doi: 10.1109/REEPE49198.2020.9059152.
- [4] A. D. J. Larminie, *Fuel Cell Systems Explained*, 2nd ed. Hoboken, NJ, USA: John Wiley & Sons, 2003.
- [5] P. H. Rodtaz, "Dynamics of the polymer electrolyte fuel cell: experiments and model-based analysis," Ph.D. dissertation, Swiss Federal Institute of Technology, Zurich, Switzerland, 2003.
- [6] B. Gou, W. Na, and B. Diong, *Fuel cells: Modeling, control, and applications*, Boca Raton, FL, USA: CRC Press, 2010.
- [7] Y.-P. Yang, F.-C. Wang, H.-P. Chang, Y.-W. Ma, and B.-J. Weng, "Low power proton exchange membrane fuel cell system identification and adaptive control," *Journal of Power Sources*, vol. 164, no. 2, pp. 761–771, Feb. 2007, doi: 10.1016/j.jpowsour.2006.11.038.
- [8] J. T. Pukrushpan, A. G. Stefanopoulou, and H. Peng, "Control of fuel cell breathing," *IEEE Control Systems*, vol. 24, no. 2, pp. 30–46, Apr. 2004, doi: 10.1109/MCS.2004.1275430.
- [9] J. T. Pukrushpan, H. Peng, and A. G. Stefanopoulou, "Simulation and analysis of transient fuel cell system performance based on a dynamic reactant flow model," in *ASME International Mechanical Engineering Congress and Exposition*, Jan. 2002, pp. 637–648, doi: 10.1115/IMECE2002-32051.
- [10] W. Garcia-Gabin, F. Dorado, and C. Bordons, "Real-time implementation of a sliding mode controller for air supply on a PEM fuel cell," *Journal of Process Control*, vol. 20, no. 3, pp. 325–336, Mar. 2010, doi: 10.1016/j.jprocont.2009.11.006.
- [11] A. Guo, W. Chen, Q. Li, Z. Liu, and H. Que, "Air flow control based on optimal oxygen excess ratio in fuel cells for vehicles," *Journal of Modern Transportation*, vol. 21, no. 2, pp. 79–85, Jun. 2013, doi: 10.1007/s40534-013-0009-8.
- [12] T. C. Ma, "Research on the control of fuel cells engine system analysing and modeling," Ph.D. dissertation, Tongji University, Shanghai, China, 2007.
- [13] D. Zhou, A. Al-Durra, F. Gao, A. Ravey, I. Matraji, and M. G. Simões, "Online energy management strategy of fuel cell hybrid electric vehicles based on data fusion approach," *Journal of Power Sources*, vol. 366, pp. 278–291, Oct. 2017, doi: 10.1016/j.jpowsour.2017.08.107.
- [14] R. Touileb and A. Abbou, "Evaluation of energy management system of a hybrid energy source in EV," *International Journal of Power Electronics and Drive Systems (IJPEDS)*, vol. 14, no. 4, pp. 1911–1918, 2023, doi: 10.11591/ijpeds.v14.i4.pp1911-1918.
- [15] L. Xu, C. D. Mueller, J. Li, M. Ouyang, and Z. Hu, "Multi-objective component sizing based on optimal energy management strategy of fuel cell electric vehicles," *Applied Energy*, vol. 157, pp. 664–674, Nov. 2015, doi: 10.1016/j.apenergy.2015.02.017.
- [16] P. Thounthong and P. Sethakul, "Analysis of a Fuel Starvation Phenomenon of a PEM Fuel Cell," in *2007 Power Conversion Conference - Nagoya*, IEEE, Apr. 2007, pp. 731–738, doi: 10.1109/PCCON.2007.373048.
- [17] R. Saïssset, C. Turpin, S. Astier, and J. M. Blaquièrre, "Electricity generation starting from a fuel cell hybridised with a storage device," in *IEEE Vehicle Power and Propulsion Conference, Paris*, 2004.
- [18] H. Otmane, Y. Mouloudi, and B. Mokhtar, "Comparative analysis of cascaded fuzzy-PI controllers based-MPPT and perturb and observe MPPT in a grid-connected PV system operating under different weather and loading conditions," *International Journal of Power Electronics and Drive Systems (IJPEDS)*, vol. 10, no. 4, pp. 1986–1994, 2019, doi: 10.11591/ijpeds.v10.i4.pp1986-1994.
- [19] R. Sakthivelsamy and K. Subramanian, "Modelling and performance analysis of free body dynamics of electric vehicles," *International Journal of Power Electronics and Drive Systems (IJPEDS)*, vol. 15, no. 1, pp. 1–7, Mar. 2024, doi: 10.11591/ijpeds.v15.i1.pp1-7.
- [20] M. Nizam and M. R. A. Putra, "Analysis of lithium-ion indirect liquid cooling battery thermal management system with high discharge rate," *International Journal of Power Electronics and Drive Systems (IJPEDS)*, vol. 14, no. 3, pp. 1414–1420, Sep. 2023, doi: 10.11591/ijpeds.v14.i3.pp1414-1420.
- [21] R. Touileb and A. Abbou, "Simulation and optimization of hydrogen consumption in a fuel cell/battery hybrid vehicle," *International Journal of Power Electronics and Drive Systems (IJPEDS)*, vol. 14, no. 2, pp. 662–672, Jun. 2023, doi: 10.11591/ijpeds.v14.i2.pp662-672.
- [22] T. Sutikno and S. Padmanaban, "Integrated motor drive for vehicle electrification: a step toward a more sustainable and efficient transportation system," *International Journal of Power Electronics and Drive Systems (IJPEDS)*, vol. 14, no. 2, pp. 649–652, Jun. 2023, doi: 10.11591/ijpeds.v14.i2.pp649-652.
- [23] W. Zhou, L. Yang, Y. Cai, and T. Ying, "Dynamic programming for new energy vehicles based on their work modes Part II: Fuel cell electric vehicles," *Journal of Power Sources*, vol. 407, pp. 92–104, Dec. 2018, doi: 10.1016/j.jpowsour.2018.10.048.




- [24] P. Mercier, "Fuel Cell Vehicle (FCV) power train," *MATLAB Central File Exchange*, 2024, [Online]. Available: <https://www.mathworks.com/matlabcentral/fileexchange/33309-fuel-cell-vehicle-fcv-power-train>.
- [25] O. Tremblay and L.-A. Dessaint, "Experimental validation of a battery dynamic model for EV applications," *World Electric Vehicle Journal*, vol. 3, no. 2, pp. 289–298, Jun. 2009, doi: 10.3390/wevj3020289.

BIOGRAPHIES OF AUTHORS






Laoufi Keltoum    obtained the L.Sc. degree in electrical engineering from the University of Oran, Algeria, in 1995, and the M.S. degree in 2004 from the University of Oran, Algeria, currently a doctoral student of the Faculty of Technology, University of Béchar, Algeria. She has been teaching at Bechar University since 2004. Her main research activities focus on FACTS technology, control of electrical systems, and optimal energy distribution and stability improvement using power electronics in the framework of constraint compensation and energy optimization. She can be contacted at email: laoufi.yousfi@yahoo.fr or laoufi.yousfi@gmail.com.






Youssef Mouloudi    received the state engineer degree in electrical engineering in 2006 from the University of Bechar and the M.S. degree in 2009 from Bechar University, Algeria. He is currently a Ph.D. student of the Faculty Technology, University of Bechar, Algeria. He is working at SONELGAZ "Algerian Electrical Society" since 1995. His areas of interest are FACTS systems, power filters, applications of power electronics, and stability improvement. Correspondence address: Department Science and Technology "Electrical Engineering", Faculty of Technology, Bechar University, BP 417, 08000 Bechar, Algeria. He can be contacted at email: mouloudiyoussef@yahoo.fr or mouloudi.youcef@univ-bechar.dz.



Abdeldjebar Hazzab    secured a state engineering degree in electrical engineering from the University of Sciences and Technology of Oran (USTO), Algeria, in 1995. He furthered his academic pursuits at the Electrical Engineering Institute of USTO, obtaining a Master of Science degree in 1999, followed by a doctoral degree (Ph.D.) from the same institution in 2006. Currently, he serves as a professor of electrical engineering at the University of Bechar, Algeria, where he serves as the Director of the Research Laboratory of Control Analysis and Optimization of Electro-Energetic Systems. Additionally, he is an adjacent Professor at École de Technologie Supérieure (ETS), Université de Montréal, Canada, and a researcher at the energy intelligence research and innovation center - Cégep de Sept-Îles. His research endeavors encompass the domains of power electronics, electric drive control, and artificial intelligence, with a particular emphasis on their practical applications. He can be contacted at email: hazzab.abdeldjebar@etsmtl.ca or abdeldjebar.hazzab@gmail.com.



Abdallah Ben Abdelkader    received the L.Sc. degree in electrical engineering from Bechar University, Bechar, Algeria, in 2006 and M.Sc. degree in electrical engineering from University of Sciences and Technology of Oran (USTO) Algeria, in 2013, respectively, where he has been working toward the doctoral degree in the Department of Electrical Engineering, 2013. He is currently a research member of Smart Grids and Renewable Energies Lab, Department of Electrical Engineering, Tahri Mohammed University Bechar, Algeria. His main research activity is focused on FACTS technology, power system control, and optimal power dispatch. Faculty of Technology, Bechar University, BP 417, 08000 Bechar, Algeria. He can be contacted at email: benabdelkader.abdallah@univ-bechar.dz or abdallahbenabdelkader@yahoo.fr.